Ecotoxicology and Environmental Safety 309 (2026) 119672

Contents lists available at ScienceDirect

Ecotoxicology and Environmental Safety

journal homepage: www.elsevier.com/locate/ecoenv

People with respiratory inflammation may be at higher health risk of bioaerosols: A comparative study of air-liquid interface and submerged exposure models

Yunyun Zhang [a,b], Na Luo [a,b], Guiying Li [a,b], Zhishu Liang [a,b], Po Keung Wong [a,b], Taicheng An [a,b,*]

[a] Guangdong-Hong Kong-Macao Joint Laboratory for Contaminants Exposure and Health, Guangdong Key Laboratory of Environmental Catalysis and Health Risk Control, Institute of Environmental Health and Pollution Control, Guangdong University of Technology, Guangzhou 510006, China
[b] Guangdong Basic Research Center of Excellence for Ecological Security and Green Development, Key Laboratory of City Cluster Environmental Safety and Green Development of the Ministry of Education, School of Environmental Science and Engineering, Guangdong University of Technology, Guangzhou 510006, China

ARTICLE INFO

Edited by Dr. RENJIE CHEN

Keywords:
Pseudomonas aeruginosa bioaerosol
Air-liquid interface model
Submerged model
Airway surface liquid accumulation
Exposure microenvironment

ABSTRACT

Bioaerosols are ubiquitous presence in ambient air, and inhalation exposure to bioaerosols may be associated with a series of respiratory diseases. However, the cytotoxic mechanism of bioaerosols remains poorly understood, emphasizing need for more physiologically relevant *in vitro* exposure models that accurately simulate respiratory microenvironment. In susceptible populations with respiratory inflammation, mucus hypersecretion and airway surface liquid (ASL) accumulation are common. Herein, two exposure models were designed: an air-liquid interface (ALI) model simulating normal respiratory epithelium and a novel submerged model simulating inflamed respiratory epithelium with pathological ASL accumulation. Cytotoxicity of *Pseudomonas aeruginosa* (*P. aeruginosa*) bioaerosol was explored with the two models. *P. aeruginosa* bioaerosol exposure (10^5 and 10^6 CFU/m^3) increased apoptosis by 3.5 % and 8.8 % in submerged model, compared to 0.1 % and 2.4 % in ALI model. In submerged model, ASL accumulation resulted in mucin hypersecretion and upregulation of bacterial adhesins, enhancing *P. aeruginosa* adhesion, invasion, biofilm formation, and ultimately led to higher cytotoxicity. In ALI model, *P. aeruginosa* bioaerosol exposure caused greater increases in epithelial permeability despite exhibiting lower cytotoxicity. This disparity resulted from attenuated upregulation of intercellular junction proteins in ALI model (*vs.* submerged). Our study revealed distinct cytotoxic mechanisms of *P. aeruginosa* bioaerosols in two models, underscoring the heightened health risks of bioaerosol exposure in individuals with pre-existing respiratory inflammation.

1. Introduction

The bioaerosols are ubiquitous presence in the ambient air and pose health risks to human beings (Liang et al., 2023; Yao, 2022; Zhao et al., 2024). According to epidemiological studies, human exposure to bioaerosols is consistently associated with multiple acute and chronic respiratory diseases, including allergies, asthma, rhinitis, chronic obstructive pulmonary disease (COPD), pneumonia and lung cancer (Iqbal et al., 2024; Zhang et al., 2024). However, the mechanisms underlying bioaerosol induced toxicological outcomes are not yet fully understood.

Due to the complex and variable composition of bioaerosols, elucidating their toxicological mechanisms remains challenging (Eduard et al., 2012; Gollakota et al., 2021). Individual antigens or purified components are typically used to insight into the toxicological profile (Mack et al., 2019; Raemy et al., 2012). Thus, *Pseudomonas aeruginosa* (*P. aeruginosa*) bioaerosol is of particular concern. As a gram-negative opportunistic pathogen with minimal nutritional requirements, *P. aeruginosa* is widely present in bioaerosols and can spread *via* airborne routes (Aziz et al., 2022; Guo et al., 2023; Wang et al., 2024b). It is also a common clinical pathogen that causes respiratory infections (Cao et al., 2023; Reynolds and Kollef, 2021). *P. aeruginosa* is responsible for

* Corresponding author at: Guangdong-Hong Kong-Macao Joint Laboratory for Contaminants Exposure and Health, Guangdong Key Laboratory of Environmental Catalysis and Health Risk Control, Institute of Environmental Health and Pollution Control, Guangdong University of Technology, Guangzhou 510006, China.
E-mail address: antc99@gdut.edu.cn (T. An).

https://doi.org/10.1016/j.ecoenv.2026.119672
Received 19 September 2025; Received in revised form 31 December 2025; Accepted 31 December 2025
Available online 6 January 2026

chronic infections in patients with chronic obstructive pulmonary disease or cystic fibrosis, contributing to high morbidity and mortality (Horstmann et al., 2021; Maurice et al., 2019). Thence, this research employed *P. aeruginosa* aerosol as typical bacterial bioaerosol to explore its cytotoxic effects.

The traditional submerged exposure model, in which cells are fully immersed in culture medium, is the most commonly used *in vitro* model for assessing the toxicological profile of pollutants *in vitro*, due to its simplicity and low cost (Dong et al., 2019). However, this method fails to prevent the interactions between medium components and test substances, influencing the bioactivity and physicochemical properties of bioaerosols or particles (Chen et al., 2024; Lakhdar et al., 2022). Moreover, under physiological conditions, respiratory epithelial cells reside at the air-liquid interface (ALI), overlaid by a thin layer (5 – 30 μm) of airway surface liquid (ASL) (Panas et al., 2014; Wang et al., 2019). Consequently, the ALI exposure model provides a platform that more closely replicates the microenvironment of the healthy human airway, not only minimizing interference from the culture medium but also enabling more precise control of exposure dose.

However, in certain respiratory diseases, such as COPD, acute lung injury, and severe asthma, accumulation of ASL is a key pathological feature, with thickness reaching hundreds of micrometers (Hill et al., 2022). This creates a submerged microenvironment at the epithelial surface, which may alter host-pathogen interactions and increase susceptibility to inhaled pathogens (Rossy et al., 2023). Despite its clinical relevance, no research has systematically compared the toxicological profile of a pathogen under these two distinct conditions: the physiologically relevant ALI condition versus the disease-associated ASL-accumulated scenario. To address this gap, we developed a novel submerged exposure model, in which epithelial cells are overlaid with a small, defined volume of buffer to mimic ASL accumulation. Compared to traditional submerged models, which use excess culture medium, both the ALI model and novel submerged model provide enhanced physiological relevance.

In this study, the distinct toxicological profile of *P. aeruginosa* bioaerosols on respiratory epithelial cells were comparably investigated using two exposure models: an ALI model simulating normal respiratory epithelium, and a novel submerged model mimicking ASL accumulated respiratory epithelium. *P. aeruginosa* bioaerosols were generated and delivered to the both exposure models using a combination of aerosol nebulizer and CULTEX radial flow system. Cytotoxic effects were assessed using multiple observational indicators, including cytotoxicity, infection-related processes (such as bacterial adhesion, invasion, and biofilm formation), and disruption of epithelial permeability. By comparing these two physiologically relevant exposure scenarios, this study provided new insights into how the airway microenvironment modulates the toxicological responses to *P. aeruginosa* bioaerosols, and provided a foundation for developing advanced *in vitro* respiratory exposure models.

2. Materials and methods

2.1. Materials

Chemicals and reagents used in this study are provided in the Text S1.

2.2. Bioaerosol exposure

2.2.1. Establishment of the exposure system

An *in vitro* cellular exposure system was set up to assess the cytotoxic mechanisms of bioaerosols (Fig. S1a). This system contained three parts: (1) bioaerosol generation by 6-jet Collison nebulizer (BGI, USA), (2) pressure and humidity regulation *via* Woulff bottle and dryer (Huifen, China), (3) cellular exposure using CULTEX® Radial Flow System (Cultex, Germany). All these parts were interconnected with low-adsorption polytetrafluoroethylene pipeline. The nebulizer generated bioaerosols, which were then delivered to cell models. A HEPA filter connected the Woulfe bottle to the atmosphere to maintain ambient pressure. The cellular exposure part contains two CULTEX® Radial Flow systems, for exposure to filtered air (control) or bioaerosols (treatment), respectively. Each system contained six chambers, three were used for ALI model cell exposure and three were dedicated to submerged model cell exposure. This system served as the experimental platform for exposure studies.

2.2.2. Establishment of the two exposure models

The human bronchial epithelial cell line BEAS-2B was obtained from the Chinese Academy of Cell Resource Center (Shanghai, China). Cells were cultured in Dulbecco's Modified Eagle Medium (DMEM) supplemented with 10 % fetal bovine serum (FBS) and 1 % penicillin–streptomycin (100 U/mL and 100 μg/mL), and maintained at 37 °C in a 5 % CO_2 incubator. The cells between passages 3–10 were used for the exposure experiments.

The two *in vitro* cell exposure models were established, and detailed protocols are provided in the Text S2 and illustrated in Fig. S1b. BEAS-2B cells were seeded onto Transwell inserts (with a 12 mm diameter polyester membrane) at a density of 50,000 cells per insert and cultured under submerged conditions. Fresh medium (0.5 mL in the apical chamber and 1.0 mL in the basal chamber) was provided every 48 h. A confluent cell monolayer was observed microscopically after 48 h of culture. For the ALI exposure model, the apical medium was removed 24 h prior to bioaerosol exposure to allow the cells to maintain at the ALI before exposure. In parallel, cells designated for submerged exposure were maintained with 0.5 mL of medium in the apical chamber and incubated for 24 h under submerged conditions. Immediately before aerosol exposure, 100 μL of PBS was applied to the apical surface of the cells, resulting in a PBS layer thickness of approximately 885 μm, to simulate pathological airway surface liquid (ASL) accumulation. The permeability of FD-4 in the ALI model reached a nadir between 72 and 96 h post-seeding, subsequently increasing after 120 h (Fig. S2a). Therefore, both exposure models were fully established at 72 h post-seeding and subsequently used for bioaerosol exposure. Both exposure models were transferred to the CULTEX® Radial Flow System for bioaerosol exposure at 72 h post-seeding.

2.2.3. Generation of P. aeruginosa bioaerosols

The ubiquitous opportunistic pathogen *P. aeruginosa* was used as the model microorganism of bioaerosols. *P. aeruginosa* cultures were initially thawed and plated on nutrient agar for 16 h at 37 °C. Subsequently, a single colony was inoculated in Luria–Bertani broth to mid-exponential phase, then harvested by centrifugation at 8000 rpm. The bacterial pellet was resuspended in sterile physiological saline (0.9 % NaCl) to create suspensions of approximately 5×10^7, 5×10^6 and 5×10^5 CFU/mL, as confirmed by standard plate counting. These suspensions were immediately aerosolized using a 6-jet Collison nebulizer. The nebulizer airflow was maintained at 12 L/min. The generated bioaerosols exhibited a diameter of approximately 1–3 μm when relative humidity was controlled at 90–95 % with a dryer (Wang et al., 2024a). The concentrations of *P. aeruginosa* bioaerosols were analyzed using an Andersen six-stage impactor (Applied Technical Institute of Liaoyang, China) and an SKC BioSampler (SKC, USA). Details of the bioaerosol concentration measurements are provided in the Text S3 and Fig. S1c.

2.2.4. P. aeruginosa bioaerosol exposure

The DMEM medium supplemented with 25 mM N-2-hydroxyethylpiperazine-N-2-ethane sulfonic acid (HEPES) was supplied to each exposure chamber of CULTEX® Radial Flow System before transferring the two exposure models. A tubing pump was used to adjust the medium level to the membrane height, ensuring adequate nutrient supply. *P. aeruginosa* bioaerosols or filtered air were delivered to each chamber at a flow rate of 5.0 mL/min (with a central airflow of 1.0 L/min) using a

vacuum pump and mass flow controllers. Cells were maintained at 37 ℃ exposed for 3 h. Afterward, both exposure models were transferred to new 12-well plates with fresh medium in the basal chamber. In the submerged model, the apical PBS layer, containing deposited *P. aeruginosa* bioaerosols, was retained. Cytotoxicity, infection-related potential and epithelial permeability were then assessed after 12 h incubation.

2.3. Quantitation of mucins

The transcription levels of mucin genes (mucin 1, *MUC1*; mucin 4, *MUC4*; mucin 7, *MUC7*; mucin 13, *MUC13*; mucin 5AC, *MUC5AC* and mucin 5B, *MUC5B*) and the concentrations of mucin proteins (MUC1 and MUC5AC) in both models were determined by real-time quantitative reverse transcription PCR (RT-qPCR) and enzyme-linked immunosorbent assay (ELISA), respectively. Following establishment of the two exposure models, total RNA and protein were extracted for quantitative analysis. Detailed experimental methods of RNA isolation, RT-qPCR, and ELISA are provided in the Texts S4–S5 and primers used are listed in the Table S1.

2.4. Cytotoxicity assay

The cytotoxicity of *P. aeruginosa* bioaerosols was assessed by measuring cell viability, cell membrane permeability, the rates of necrosis and apoptosis. Cell viability was evaluated by Cell Counting kit (CCK-8). The plasma membrane integrity assay was performed by Cytotoxicity LDH Assay Kit-WST based on the activity of lactate dehydrogenase (LDH) in the medium. Necrotic and apoptotic cells were identified using an Annexin V-FITC Apoptosis Detection Kit. Detailed experimental procedures are provided in the Text S6.

2.5. Adhesion and invasion assay

Adhesion refers to the attachment of bacteria to host cells, while invasion describes the internalization of bacteria into BEAS-2B cells. These processes were quantified through bacterial enumeration and RT-qPCR analysis of adhesin genes (type IV pilus assembly ATPase PilB, *pilB*; type IV pilus assembly protein PilM, *pilM*; flagellar motor switch protein FliM, *fliM* ; flagellar type III secretion system protein FliP, *fliP* and c-di-GMP phosphodiesterase CdrB, *cdrB*). For the adhesion assay, BEAS-2B cells were washed three times with PBS to remove the non-adherent bacteria. Following 10 min lysis with 0.1 % SDS, *P. aeruginosa* colony-forming units (CFU) were quantified by serial dilution and plating. For invasion assays, following PBS washes, the cells were cultured with medium containing 25 μg/mL gentamicin for 1 h before 0.1 % SDS lysis. The bactericidal efficacy of gentamicin was confirmed in preliminary experiments (Fig. S2b). The number of invading *P. aeruginosa* CFUs were then quantified by serial dilution and plating. Moreover, the expression levels of adhesin related genes were analyzed using RT-qPCR, as detailed in Text S4. The primers used are listed in the Table S1.

2.6. Evaluation of biofilm formation

Biofilm formation was evaluated using two methods: crystal violet staining and scanning electron microscopy (SEM). After bioaerosol exposure, non-adherent bacteria were removed by washing with PBS. Adherent biofilms were fixed with 100 μL 4 % paraformaldehyde for 10 min and air-dried. They were then stained for 5 min with 200 μL 1 % crystal violet, after which excess stain was rinsed off with PBS. The air-dried cell exposure models were treated with 200 μL 33 % (v/v) glacial acetic acid to dissolve the crystal violet. The optical density (OD) was assessed at 590 nm using a microplate reader.

For SEM imaging, both cell exposure models were washed with PBS to remove the non-adherent bacteria. Then, the cells were fixed with 2.5 % glutaraldehyde for 1 h at 4 °C and dehydrated through a graded ethanol series (30 %, 50 %, 70 %, 80 %, 90 %, and 100 % × 2), with each step lasting 5 min. Samples were stored in a desiccator until sputter-coated with gold–palladium for 100 s. Biofilm imaging was carried out using TESCAN CLARA electron microscope at 2 kV.

2.7. Determination of epithelial permeability

Epithelial permeability was measured by using 4 kDa fluorescein isothiocyanate-dextran (FITC-dextran, FD-4). Following bioaerosol exposure, cell exposure models were washed with PBS for three times. Then, 500 μL of phenol red-free DMEM was added to the basolateral chamber of the Transwell inserts, and 500 μL of phenol red-free DMEM containing 0.5 mg/mL FD-4 was added to apical chamber. Then the exposure models were cultured for 1.5 h at 37 °C. FD-4 concentrations were subsequently quantified using a microplate reader with excitation and emission wavelengths of 485 and 535 nm, respectively.

Bacterial penetration of the epithelial barrier was also evaluated. After exposure, basolateral medium was collected, serially diluted, and plated on agar to determine CFUs. Penetration rates were calculated as the ratio of CFU in the basolateral medium.

Further, the expression levels of cell junction-related genes (occludin, *OCLN*; claudin-1, *CLDN1*; integrin β1, *ITGB1*; cadherin 1, *CDH1*; desmoplakin, *DSP*; junction plakoglobin, *JUP*; vinculin, *VCL*; fibronectin 1, *FN1* and laminin subunit gamma, *LAMC*) were analyzed by RT-qPCR. Total RNA was extracted from BEAS-2B cells after bioaerosol exposure. Detailed experimental methods of RNA isolation, RT-qPCR are provided in the Text S4 and primers used are listed in the Table S1.

2.8. Statistical analysis

The data are expressed as mean ± standard deviation of three independent experiments. Statistical analysis and graphic presentation were performed using GraphPad Prism 7.0 software. Statistical analyses employed unpaired *t*-test for mucin quantification (RT-qPCR/ELISA) between two exposure models, and Two-way ANOVA was employed in bioaerosol exposure outcome analysis, including cytotoxicity, infection-related processes and epithelial permeability. Differences with p-values < 0.05 are considered to be significant.

3. Results and discussion

3.1. Establishment and characterization of the two exposure models

The ALI exposure model and novel submerged exposure model were established utilizing the Transwell inserts supported by polyester membrane. BEAS-2B cells served as the target cells due to their ability to express junction proteins and secrete mucins (Liu et al., 2020; Zhang et al., 2021). In the ALI model, the apical medium was removed 48 h post-seeding, and the cells were maintained at the ALI for 24 h before exposure. For the novel submerged model, 100 μL of PBS was applied to the apical surface of ALI model before exposure, simulating the ASL layer (Fig. S1b) (Tavana et al., 2010). In contrast to traditional submerged models that use complex, protein-rich culture media, where bioaerosols may aggregate, adsorb, or altered bioactivity, the novel submerged model utilizes an isotonic buffer with minimal components, significantly reducing matrix interference, and simulating the ionic milieu of ASL.

The ASL is primarily composed of water (~ 95 %), electrolytes, mucins, and antimicrobial substances (Abrami et al., 2024). To accurately compare the microenvironment simulated by these two models, we quantified mucin expression. Fig. 1a shows that the novel submerged model exhibited significantly higher mucin gene transcription levels, ranging from 1.6- to 3.2-fold greater than those in the ALI model. Specifically, the relative expression levels of *MUC1*, *MUC4*, *MUC7*, *MUC13*, *MUC5AC*, and *MUC5B* in the ALI model were only 68 %, 24 %,

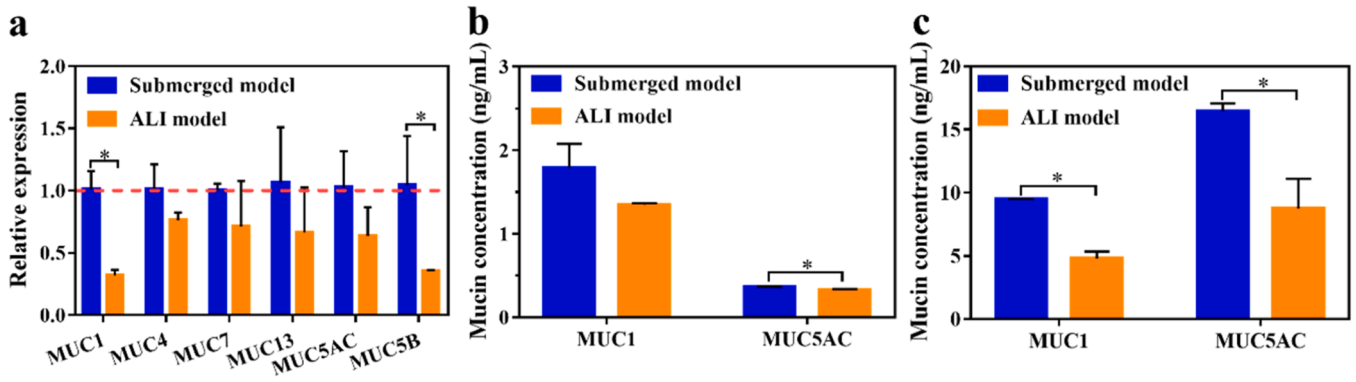

Fig. 1. Mucin levels in two exposure models. (a) Mucin gene expressions in BEAS-2B cells cultured under submerged and ALI models, respectively. (b) Intracellular concentrations of MUC1 and MUC5AC in BEAS-2B cells cultured under submerged and ALI models, respectively. (c) Extracellular concentrations of MUC1 and MUC5AC in BEAS-2B cells cultured under submerged and ALI models, respectively. Asterisks (*) denote statistically significant differences between the two groups, as determined by an unpaired *t*-test.

29 %, 33 %, 36 %, and 64 %, respectively, of those in the submerged model. Among them, *MUC1* and *MUC5B* showed statistically significant upregulation. Furthermore, the protein levels of typical mucins, MUC1 and MUC5AC, were quantified by ELISA. As shown in Fig. 1b, in the submerged model, intracellular MUC1 and MUC5AC concentrations were 1.3- and 1.1-fold higher than those in the ALI model, respectively. Extracellular concentrations were 2.0- and 1.9-fold higher, respectively (Fig. 1c). These extracellular increases were statistically significant and more pronounced than the intracellular differences, which is consistent with the secretory nature of MUC1 and MUC5AC as extracellular mucins. Collectively, significantly elevated mucin production and secretion in the novel submerged model compared to the ALI model were confirmed by both RT-qPCR and ELISA. The increased mucin secretion and the presence of a fluid buffer layer in the novel submerged model recapitulate key features of pathological ASL accumulation, supporting its relevance as a model for ASL accumulated microenvironment.

The ALI model is widely recognized as a physiologically relevant platform for simulating the normal respiratory microenvironment. However, many respiratory diseases are accompanied by pathological ASL accumulation. ASL accumulation creates a fluid-covered microenvironment that facilitates pathogen adhesion, colonization, and infection, underscoring the necessity of this novel submerged model. Although PBS lacks the full biochemical complexity of native ASL, this simplified submerged model partially recapitulates the key features of ASL accumulation, particularly the physical presence of a fluid layer and mucus hypersecretion. Furthermore, the liquid layer can create an oxygen gradient distinct from the ALI condition, partially simulating the hypoxic microenvironment resulting from impaired gas diffusion in ASL-thickened regions. Although a true diseased airway involves additional factors, such as chronic inflammation, immune cell infiltration, and sustained hypoxia, the submerged model provides a disease-relevant platform for studying the impact of ASL accumulation on host–pathogen interactions.

3.2. Cytotoxicity of *P. aeruginosa* bioaerosols in two different exposure models

P. aeruginosa bioaerosols were generated using a 6-jet Collision nebulizer (Fig. S1a). This nebulizer produced bioaerosols from *P. aeruginosa* suspensions at concentrations of 5×10^7, 5×10^6, and 5×10^5 CFU/mL at a flow rate of 12 L/min. The resultant concentrations of *P. aeruginosa* bioaerosols were 9.7×10^6, 1.9×10^5, 6.0×10^4 CFU/m^3 detected with SKC BioSampler (Fig. S3a) and 2.1×10^6, 4.7×10^4, 5.3×10^3 CFU/m^3 detected with Andersen six-stage impactor (Fig. S3b), respectively. Comparable trends were obtained with both sampling methods, demonstrating the stability of *P. aeruginosa* bioaerosol generation. Andersen six-stage impactor was a widely used sampler for bioaerosols collection, yet its detection range is limited (Nguyen et al., 2022). Therefore, the concentration measured by SKC BioSampler 9.7×10^6 CFU/m^3 (briefly describes as 10^6 CFU/m^3 in following text) and 1.9×10^5 CFU/m^3 (briefly describes as 10^5 CFU/m^3 in following text) were used as a reference. Generally, ambient bacterial aerosol concentrations typically ranges from 10^3 to 10^5 CFU/m^3 (Liang et al., 2020). In certain scenarios, such as haze events or aquaculture conditions, the bacterial abundance can reach 10^5–10^6 CFU/m^3 (Saikh and Das, 2023). Therefore, in this study, 10^5 and 10^6 CFU/m^3 *P. aeruginosa* bioaerosols were used to simulate bacterial aerosol exposure at high environmental concentrations, with filtered air serving as the control.

The cytotoxicity of *P. aeruginosa* bioaerosols was comparatively assessed using the two exposure models. A significant and concentration-dependent reduction in cell viability was observed after 3 h exposure in both models. Specifically, in the submerged model, exposure to 10^5 and 10^6 CFU/m^3 *P. aeruginosa* bioaerosols increased the apoptotic cell rate from 2.1 % to 5.6 % and 10.9 %, respectively, and the necrotic cell rate from 5.4 % to 8.0 % and 17.5 %, respectively (Fig. 2a–c). Cytotoxicity of *P. aeruginosa* bioaerosol was further assessed by measuring mitochondrial dehydrogenase activity and membrane permeability. Exposure to 10^6 CFU/m^3 *P. aeruginosa* bioaerosol resulted in 48.3 % reduction in cell viability and 114.1 % increase in the LDH release under submerged model (Figs. 3a and 3b). In ALI model, exposure to the same concentration *P. aeruginosa* bioaerosol, the apoptosis rate increased from 4.5 % to 4.6 % and 6.9 %, respectively, and the necrotic rates increased from 8.2 % to 9.9 % and 11.4 %, respectively (Fig. 2a–c). Exposure to 10^6 CFU/m^3 *P. aeruginosa* bioaerosol caused 34.0 % reduction in cell viability and 45.5 % increase in the LDH release (Figs. 3a and 3b). Overall, submerged exposure to *P. aeruginosa* bioaerosols induced significantly greater cytotoxicity than ALI exposure, verifying by higher levels of cell apoptosis, necrosis, membrane damage, and reduced metabolic activity.

While few researches focused on the cytotoxicity of bacterial aerosols, previous studies have compared the cytotoxicity and inflammatory responses of pollutants, such as nanoparticles and $PM_{2.5}$, under ALI versus traditional submerged exposure conditions (Dong et al., 2019; Panas et al., 2014). These studies demonstrated that differing levels of cell damage were observed under the two different exposure modes, highlighting the critical role of the microenvironment in pollutant toxicity assessment, confirmed by this study. Respiratory inflammation is often accompanied by ASL accumulation and mucus hypersecretion, conditions known to increase the risk of pulmonary infections (Bustos et al., 2023; Kumar et al., 2021). To model this pathological state, a novel submerged model that simulates the exposure microenvironment

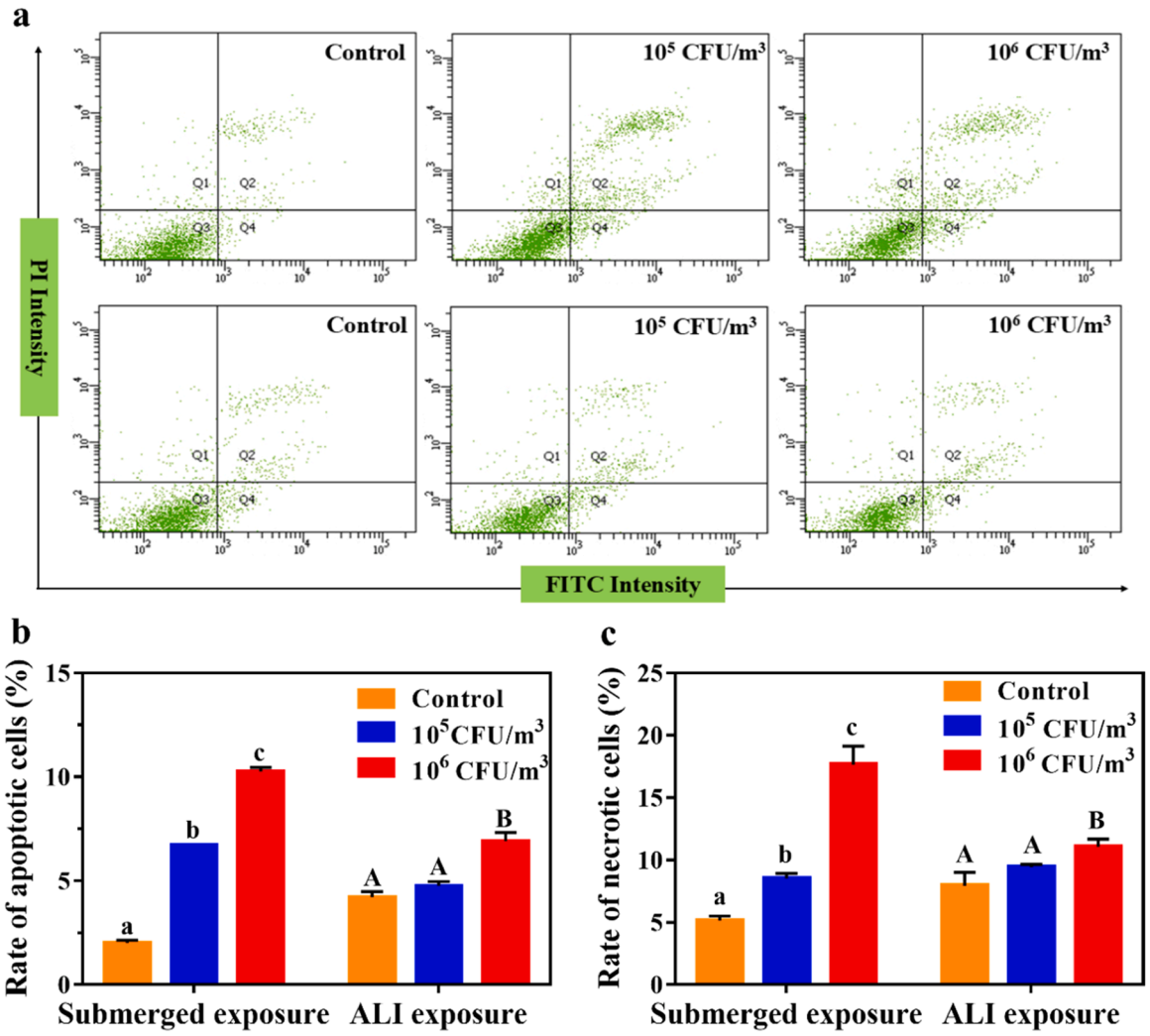

Fig. 2. Apoptotic and necrotic of BEAS-2B cells after 3 h exposure to *P. aeruginosa* bioaerosols under submerged and ALI models, respectively. (a) Representative flow cytometry scatter plots showing the apoptotic and necrotic ratios in BEAS-2B cells. (b) Quantification statistics of apoptotic ratio in BEAS-2B cells. (c) Quantification statistics of necrotic ratio in BEAS-2B cells. Different letters above the bars indicate statistically significant differences between groups ($p < 0.05$), as determined by Two-way ANOVA.

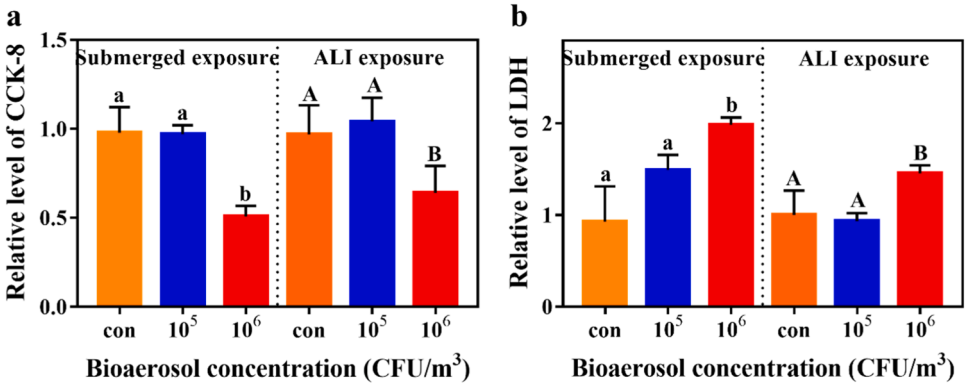

Fig. 3. Cell viability and membrane permeability of BEAS-2B cells after *P. aeruginosa* bioaerosols exposure under submerged and ALI models, respectively. (a) Cell viability of BEAS-2B cells after 0 CFU/m^3 (con, orange), 10^5 CFU/m^3 (blue), 10^6 CFU/m^3 *P. aeruginosa* bioaerosols exposure under submerged and ALI models, respectively. (b) Membrane permeability of BEAS-2B cells after 0 CFU/m^3 (con, orange), 10^5 CFU/m^3 (blue), 10^6 CFU/m^3 *P. aeruginosa* bioaerosols exposure under submerged and ALI models, respectively. Different letters above the bars indicate statistically significant differences between groups ($p < 0.05$), as determined by Two-way ANOVA.

characterized by accumulated ASL and mucin hypersecretion was developed. Our results demonstrate that the cells within this disease-relevant microenvironment exhibit heightened susceptibility to *P. aeruginosa* bioaerosols, aligning with the increased infection risk

observed in patients with respiratory diseases.

3.3. Distinct cytotoxic mechanisms in two different exposure models

Adhesion, invasion and biofilm formation constitute key virulence-associated phenotypes that determine *P. aeruginosa* infection dynamics, the process by which the pathogen breaches host defenses and colonizes host cells and tissues (Borkar et al., 2013; Nie et al., 2022). To account for the differential cytotoxicity observed between the two exposure models, we comparatively assessed *P. aeruginosa* bioaerosol adhesion, invasion, and biofilm formation to quantify the infection dynamics. Submerged exposure to 10^5 and 10^6 CFU/m^3 *P. aeruginosa* bioaerosols resulted in 3.5×10^7 and 9.6×10^7 CFU/insert of adherent bacteria, respectively (Fig. 4a). The corresponding invading bacteria were obtained as 3.3×10^2 and 9.4×10^3 CFU/insert under submerged exposure (Fig. 4b). To verify the adhesion capacity of *P. aeruginosa* bioaerosols, the expression adhesin related genes in *P. aeruginosa* was quantified by RT-qPCR. Compared to planktonic *P. aeruginosa,* the relative transcription levels of *pilB*, *pilM*, *fliM*, *fliP*, and *cdrB* in bacteria exposed to the ALI model were significantly downregulated to 0.4 ± 0.1, 0.1 ± 0.01, 0.4 ± 0.03, 0.3 ± 0.03, and 0.4 ± 0.02 folds, respectively (Fig. 4c).

While in the ALI model, exposure to *P. aeruginosa* bioaerosols at 10^5 and 10^6 CFU/m^3 resulted in 5.6×10^6 and 5.8×10^6 CFU/insert of adherent bacteria, and 4.1×10^2 and 4.1×10^3 CFU/insert invading bacteria, respectively (Figs. 4a and 4b). Compared to planktonic *P. aeruginosa* controls, the corresponding relative transcription levels of *pilB, pilM, fliM, fliP, and cdrB* in bacteria exposed under submerged model were 0.7 ± 0.1, 0.1 ± 0.02, 0.5 ± 0.1, 0.5 ± 0.03, and 0.4 ± 0.1 -fold, respectively (Fig. 4c). Submerged exposure induced significantly higher adhesin gene expression than those observed in ALI model. The upregulation of adhesin expression resulted in enhanced adhesion and invasion of *P. aeruginosa* bioaerosols in the submerged model. Bacterial adhesion was approximately 10-fold greater under submerged model than in the ALI model at both bioaerosol concentrations tested. Given the fundamental role of adhesion in the invasion process, the increased invasion is likely attributable to upregulated adhesin expression. *P. aeruginosa*, while ubiquitous, exhibits greater adaptation to soil and aquatic environments than to atmospheric ones (Ambreetha and Singh, 2023). Accumulated ASL, with up to 90 % water content, created a more suitable environment for bacterial infection. In both models, aerosolized *P. aeruginosa* showed reduced adhesin expression (relative expression levels < 1) compared to planktonic bacteria, supporting the hypothesis. The fluid-covered submerged model may enhance bacterial fitness, thereby promoting increased adhesion, invasion, and biofilm formation.

Adhesins not only mediate the adhesion to host cells, but also contribute to the biofilm formation. Therefore, we investigated *P. aeruginosa* biofilm formation under two different models. Fig. 4d shows that submerged exposure to 10^5 and 10^6 CFU/m^3 *P. aeruginosa* bioaerosols resulted in biofilm formation at 91.8 % and 114.6 % of the control, respectively. Optical microscope and SEM were utilized to visualize these findings more directly. Cells exposed to filtered air displayed clear boundaries and intact morphology (Figs. 5a and 5d). After submerged exposure to *P. aeruginosa* bioaerosols, a sheet-like covering (Figs. 5e and 5f) and agglomerated bacterial clusters (Figs. S4 and S5), consistent with biofilm morphology, were observed on the host cell surface.

Under the ALI model, biofilm biomasses were 78.4 % and 99.7 % of

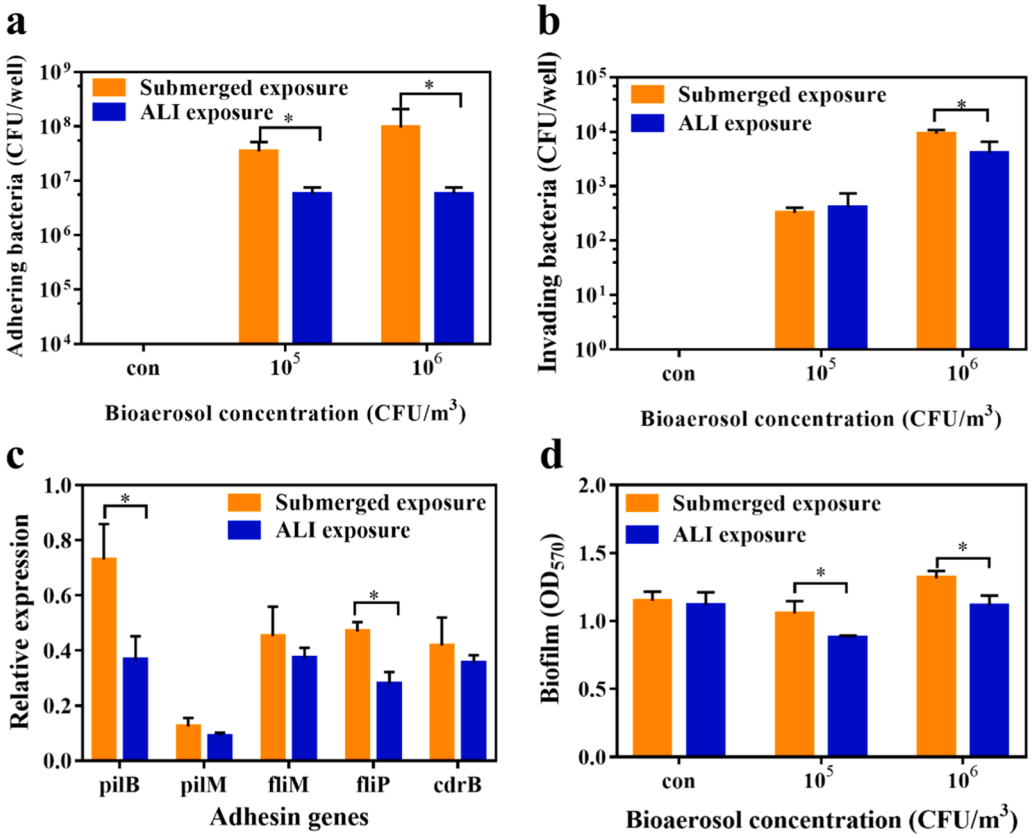

Fig. 4. The infection dynamics of *P. aeruginosa* after bioaerosol exposure under submerged and ALI models, respectively. (a) Adhesion of *P. aeruginosa* after bioaerosol exposure under submerged and ALI models, respectively. (b) Invasion of *P. aeruginosa* after bioaerosol exposure under submerged and ALI models, respectively. (c) The expressions of adhesin genes of *P. aeruginosa* bioaerosols under submerged and ALI models, respectively. (d) Biofilm formation under submerged and ALI models respectively with crystal violet staining. Asterisks (*) denote statistically significant differences between the two groups, as determined by Two-way ANOVA.

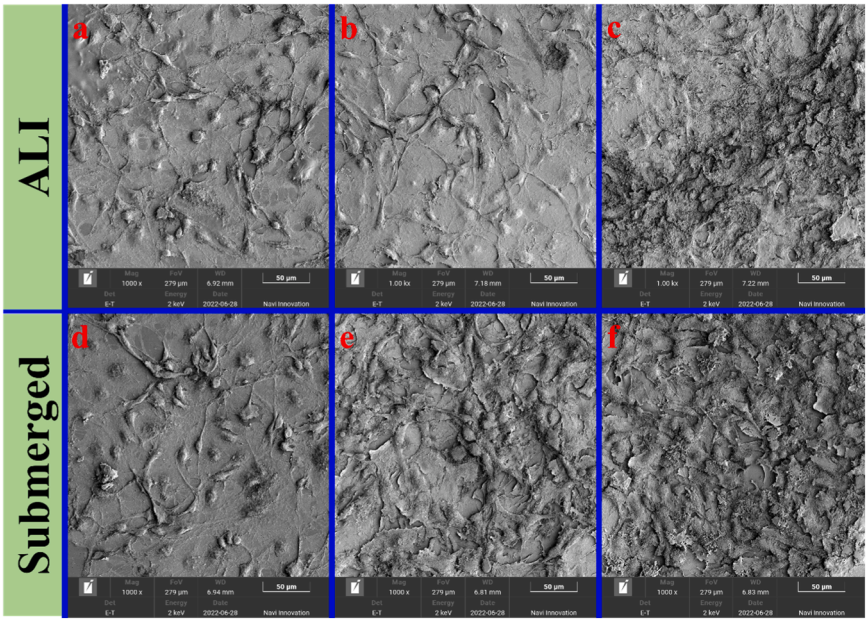

Fig. 5. SEM images of BEAS-2B cells after *P. aeruginosa* bioaerosols exposure. (a) SEM images of BEAS-2B cells after filtered air exposure under ALI model. (b) SEM images of BEAS-2B cells after 10^5 CFU/m^3 *P. aeruginosa* bioaerosols exposure under ALI model. (c) SEM images of BEAS-2B cells after 10^6 CFU/m^3 *P. aeruginosa* bioaerosols exposure under ALI model. (d) SEM images of BEAS-2B cells after filtered air exposure under submerged model. (e) SEM images of BEAS-2B cells after 10^5 CFU/m^3 *P. aeruginosa* bioaerosols exposure under submerged model. (f) SEM images of BEAS-2B cells after 10^6 CFU/m^3 *P. aeruginosa* bioaerosols exposure under submerged model.

the control after exposure to 10^5 and 10^6 CFU/m^3 *P. aeruginosa* bioaerosols, respectively (Fig. 4d). Microscope images revealed no significant biofilm formation under ALI model; however, extensive cell shedding was observed (Figs. 5b, 5c, and S4). Crystal violet staining reflects the total biomass of cells and bacteria in the exposure models. The reduced staining intensity in *P. aeruginosa* exposed groups likely results from cytotoxicity-induced cell death and subsequent detachment from Transwell inserts. Although inducing higher cytotoxicity, submerged exposure resulted in significantly greater biofilm biomass than ALI exposure, with 20.5 % and 18.2 % increase under 10^5 and 10^6 CFU/m^3 *P. aeruginosa* bioaerosol exposure, respectively. In submerged model, upregulated bacterial adhesins promoted bacterial adhesion, invasion and biofilm formation of *P. aeruginosa* bioaerosol, key drivers of elevated cytotoxicity compared to ALI models. Crucially, biofilm development not only bolsters bacterial resistance to host clearance mechanisms but also promotes chronic infections. ASL exerts a dual role in antimicrobial defense: its antimicrobial substances facilitate pathogen clearance, whereas pathological ASL accumulation promotes adhesin and mucin expression, as well as bacterial biofilm formation, thereby increasing susceptibility to chronic infections.

Optical microscope and SEM images (Figs. 5b, 5c, and S4) showed significant cell shedding in the ALI model following exposure to *P. aeruginosa* bioaerosol, suggesting an increase in epithelial permeability. To confirm this phenomenon, the FD-4 and bacterial permeability across the polarized epithelial monolayer in both models was measured. Following submerged exposure to 10^5 and 10^6 CFU/m^3 *P. aeruginosa* bioaerosols, FD-4 permeability increased by 24.9 % and 39.0 %, respectively (Fig. 6a), and the bacteria penetrate to the basolateral chamber reached 1.5×10^5 and 2.5×10^5 CFU/insert, respectively (Fig. 6b). In the ALI model at the same exposure concentration, FD-4 permeability increased by 31.9 % and an 82.4 % increase (Fig. 6a), and bacterial permeability reached 2.2×10^5 and 3.7×10^5 CFU/insert, respectively (Fig. 6b). In the ALI model, FD-4 permeability was 1.1–1.4 times higher, and the bacterial translocation was approximately 1.5 times greater, than in the submerged model, indicating markedly elevated paracellular permeability in the ALI model.

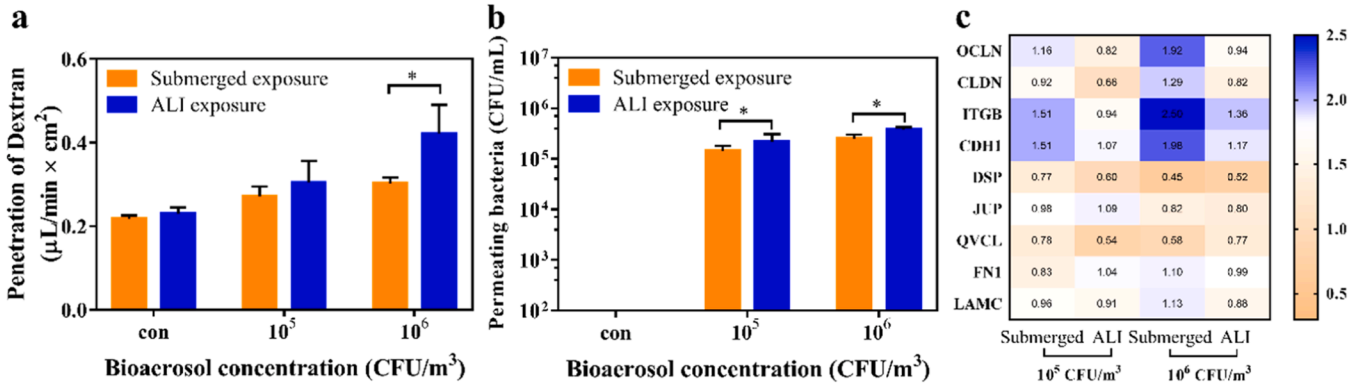

Fig. 6. The permeability of epithelial barrier after *P. aeruginosa* bioaerosols exposure under submerged and ALI models. (a) The permeability of epithelial barrier to FD-4. (b) The permeability of epithelial barrier to *P. aeruginosa*. (c) The expression of genes related to cell junction proteins. Asterisks (*) denote statistically significant differences between the two groups, as determined by Two-way ANOVA.

The airway epithelium regulates paracellular permeability through the collaboration of epithelial cells and intercellular junctions, wherein cell viability and intercellular junction integrity are critical for maintaining the permeability homeostasis of the polarized epithelial monolayer (Herrero et al., 2018). Comparing to submerged model, exposure to *P. aeruginosa* bioaerosols in ALI model primarily increased epithelial permeability, rather than induced direct cytotoxicity. Therefore, the disruption of intercellular junctions subsequently verified by examining the expression of intercellular junction-related genes. In the submerged model, exposure to 10^5 CFU/m^3 resulted in following relative transcript levels versus filtered air control: 1.2, 0.9, 1.5, 1.5, 0.8, 1.0, 0.8, 0.8, and 1.0 for *OCLN*, *CLDN*, *ITGB*, *CDH1*, *DSP*, *JUP*, *VCL*, *FN1*, and *LAMC*, respectively (Fig. 6c). Exposure to 10^6 CFU/m^3 yielded relative transcript levels of 1.9, 1.3, 2.5, 2.0, 0.5, 0.8, 0.6, 1.1, and 1.1, respectively (Fig. 6c). In the ALI model, 10^5 CFU/m^3 *P. aeruginosa* bioaerosols exposure resulted in relative transcript levels of 0.8, 0.7, 0.9, 1.1, 0.6, 1.0, 0.5, 1.0, and 0.9, respectively, while 10^6 CFU/m^3 exposure yielded relative transcript levels of 0.9, 0.8, 1.4, 1.2, 0.5, 0.8, 0.8, 1.0, and 0.9, respectively (Fig. 6c). Following exposure to *P. aeruginosa* bioaerosol, upregulation of genes encoding tight junction proteins (OCLN, CLDN) and anchored transmembrane components (CDH1, ITGB) was observed, indicating a potential host repair response. Conversely, the expression of intracellular anchoring protein (DSP, JUP, and VCL) were downregulated, while extracellular matrix component (FN1, LAMC1) remained largely unchanged. The host repair response to *P. aeruginosa* bioaerosol was attenuated in the ALI model than in the submerged model. Specifically, upregulation of tight junction and anchored transmembrane proteins were all less pronounced in the ALI model. This diminished repair response of junctional components likely contributed to greater increase in paracellular permeability observed in the ALI model. Elevated epithelial permeability compromises lung barrier function, enabling bacteria to translocate across alveolar walls into the bloodstream and trigger systemic infection (Ruenraromgsak et al., 2016).

P. aeruginosa bioaerosols induced distinct cytotoxic mechanisms in the two exposure models. In submerged model, upregulated adhesin expression enhanced bacterial adhesion, invasion and biofilm formation of *P. aeruginosa* bioaerosols, leading to increased cytotoxicity. In ALI model, the attenuated host repair response, characterized by diminished upregulation of tight junction and anchored transmembrane components, resulted in greater paracellular permeability and enhanced bacterial translocation. These findings highlight the importance of exposure microenvironment: a small volume of buffer significantly altered the expression of bacterial adhesins, mucin and intercellular junctions in cellular models. This necessitates exposure models that more precisely simulate *in vivo* conditions, whether normal respiratory epithelium or epithelium with pathological ASL accumulation, to accurately elucidate physiological response mechanisms.

4. Conclusions

In this study, we designed and compared two distinct exposure models to assess cytotoxic effects of *P. aeruginosa* bioaerosol. The ALI model used for simulating normal respiratory epithelium, while the novel submerged exposure model mimicked the pathological respiratory characterized by ASL accumulation. In submerged model, ASL accumulation not only replicated the mucus hypersecretion characteristic of respiratory inflammation, but also upregulated bacterial adhesins, thereby promoting *P. aeruginosa* adhesion, invasion and biofilm formation, and ultimately leading to enhanced cytotoxicity. The ALI model exhibited attenuated upregulation of tight junction (OCLN, CLDN) and anchored transmembrane components (CDH1, ITGB), resulting in greater paracellular permeability and increased bacterial permeability. The distinct cytotoxic mechanisms observed between the two exposure models highlight the decisive influence of exposure microenvironments on host-pathogen interactions. These findings provide mechanistic insights into the infection dynamics of *P. aeruginosa* bioaerosols and highlight the elevated health risks posed by bioaerosol exposure in individuals with respiratory disease.

5. Limitations

However, a key limitation lies in the use of PBS to simulate ASL accumulation. This approach significantly simplified the in vivo airway microenvironment. However, native ASL is a complex biological fluid containing mucins, antimicrobial peptides, inflammatory mediators, and immune components. Moreover, PBS does not recapitulate the altered oxygen tension often present in diseased airways with ASL accumulation. Additionally, the presence of PBS layer on the apical surface may influence aerosol deposition dynamics. Second, the ALI model was established by removing apical medium 24 h prior to exposure, whereas the submerged model was maintained with apical medium throughout the culture period. This difference likely resulted in divergent basal states of epithelial differentiation and gene expression. Consequently, the observed differences in cytotoxic responses to *P. aeruginosa* bioaerosols may reflect a combination of pre-existing cellular phenotypes and exposure conditions. Third, BEAS-2B cells, while useful for mechanistic studies, do not form a high-resistance epithelial barrier. Therefore, measurements of FD-4 flux and bacterial translocation should not be interpreted as indicators of "intact barrier function" but rather as relative changes in paracellular permeability under experimental conditions. Despite these limitations, our findings provide valuable insights into how microenvironment modulates host–pathogen interactions. Future advancements in ASL representation, microfluidic technology and the adoption of primary airway epithelial cells will enhance the physiological relevance of *in vitro* exposure models.

CRediT authorship contribution statement

Na Luo: Methodology, Data curation. **Yunyun Zhang:** Writing – original draft, Methodology, Investigation, Formal analysis. **Guiying Li:** Writing – review & editing, Funding acquisition, Conceptualization. **Po Keung Wong:** Supervision, Conceptualization. **Zhishu Liang:** Visualization, Methodology. **Taicheng An:** Writing – review & editing, Supervision, Funding acquisition, Conceptualization.

Declaration of Competing Interest

The authors declare that they have no known competing financial interests or personal relationships that could have appeared to influence the work reported in this paper.

Acknowledgement

This work was supported by National Key Research and Development Project (2023YFC3708204 and 2023YFC3708202), the National Natural Science Foundation of China (U25A20814 and 42130611), and Introduction Innovative and Research Teams Project of Guangdong Pearl River Talents Program (2023ZT10L102).

Appendix A. Supporting information

Supplementary data associated with this article can be found in the online version at doi:10.1016/j.ecoenv.2026.119672.

Data availability

All data generated during this study are included in this published article and its supplementary information files.

References

Abrami, M., Biasin, A., Tescione, F., Tierno, D., Dapas, B., Carbone, A., Grassi, G., Conese, M., Di Gioia, S., Larobina, D., Grassi, M., 2024. Mucus structure, viscoelastic properties, and composition in chronic respiratory diseases. Int. J. Mol. Sci. 25, 1933.

Ambreetha, S., Singh, V., 2023. Genetic and environmental determinants of surface adaptations in *Pseudomonas aeruginosa*. Microbiology-SGM 169, 001335.

Aziz, S., Mahmoud, R., Mohamed, M.B.E., 2022. Control of biofilm-producing *Pseudomonas aeruginosa* isolated from dairy farm using Virokill silver nano-based disinfectant as an alternative approach. Sci. Rep. 12, 9452.

Borkar, D.S., Fleiszig, S.M.J., Leong, C., Lalitha, P., Srinivasan, M., Ghanekar, A.A., Tam, C., Li, W.Y., Zegans, M.E., McLeod, S.D., Lietman, T.M., Acharya, N.R., 2013. Association between cytotoxic and invasive *Pseudomonas aeruginosa* and clinical outcomes in bacterial keratitis. JAMA Ophthalmol. 131, 147–153.

Bustos, N.A., Ribbeck, K., Wagner, C.E., 2023. The role of mucosal barriers in disease progression and transmission. Adv. Drug Deliv. Rev. 200, 115008.

Cao, P.B., Fleming, D., Moustafa, D.A., Dolan, S.K., Szymanik, K.H., Redman, W.K., Ramos, A., Diggle, F.L., Sullivan, C.S., Goldberg, J.B., Rumbaugh, K.P., Whiteley, M., 2023. A *Pseudomonas aeruginosa* small RNA regulates chronic and acute infection. Nature 618, 358–364.

Chen, S.S., Zhang, Y.X., Chen, H.J., Zheng, W.J., Hu, X., Mao, L., Guo, X.W., Lian, H.Z., 2024. Surface property and *in vitro* toxicity effect of insoluble particles given by protein corona: Implication for PM cytotoxicity assessment. Eco-Environ. Health 3, 137–144.

Dong, H., Zheng, L., Duan, X., Zhao, W., Chen, J., Liu, S., Sui, G., 2019. Cytotoxicity analysis of ambient fine particle in BEAS-2B cells on an air-liquid interface (ALI) microfluidics system. Sci. Total Environ. 677, 108–119.

Eduard, W., Heederik, D., Duchaine, C., Green, B.J., 2012. Bioaerosol exposure assessment in the workplace: the past, present and recent advances. J. Environ. Monit. 14, 334–339.

Gollakota, A.R.K., Gautam, S., Santosh, M., Sudan, H.A., Gandhi, R., Jebadurai, V.S., Shu, C.M., 2021. Bioaerosols: characterization, pathways, sampling strategies, and challenges to geo-environment and health. Gondwana Res. 99, 178–203.

Guo, J.J., Wang, B.J., Qiu, X., Ren, S.J., Wang, Y.K., 2023. Improvement of chlorination and sterilization of pathogenic bacteria by natural products. J. Hazard. Mater. Adv. 10, 100318.

Herrero, R., Sanchez, G., Lorente, J.A., 2018. New insights into the mechanisms of pulmonary edema in acute lung injury. Ann. Transl. Med. 6, 32.

Hill, D.B., Button, B., Rubinstein, M., Boucher, R.C., 2022. Physiology and pathophysiology of human airway mucus. Physiol. Rev. 102, 1757–1836.

Horstmann, J.C., Laric, A., Boese, A., Yildiz, D., Röhrig, T., Empting, M., Frank, N., Krug, D., Müller, R., Schneider Daum, N., de Souza Carvalho Wodarz, C., Lehr, C.M., 2021. Transferring microclusters of *P. aeruginosa* biofilms to the air-liquid interface of bronchial epithelial cells for repeated deposition of aerosolized tobramycin. ACS Infect. Dis. 8, 137–149.

Iqbal, M.A., Siddiqua, S.A., Faruk, M.O., Islam, A.M.T., Salam, M.A., 2024. Systematic review and meta-analysis of the potential threats to respiratory health from microbial Bioaerosol exposures. Environ. Pollut. 341, 122972.

Kumar, P., Singh, A.B., Singh, R., 2021. Seasonal variation and size distribution in the airborne indoor microbial concentration of residential houses in Delhi and its impact on health. Aerobiologia 37, 719–732.

Lakhdar, R., Mumby, S., Abubakar-Waziri, H., Porter, A., Adcock, I.M., Chung, K.F., 2022. Lung toxicity of particulates and gaseous pollutants using *ex-vivo* airway epithelial cell culture systems. Environ. Pollut. 305, 119323.

Liang, Z., Yu, Y., Ye, Z., Li, G., Wang, W., An, T., 2020. Pollution profiles of antibiotic resistance genes associated with airborne opportunistic pathogens from typical area, Pearl River Estuary and their exposure risk to human. Environ. Int. 143, 105934.

Liang, Z., Yu, Y., Wang, X., Liao, W., Li, G., An, T., 2023. The exposure risks associated with pathogens and antibiotic resistance genes in bioaerosol from municipal landfill and surrounding area. J. Environ. Sci. 129, 90–103.

Liu, Y., Zhou, T., Sun, L.Y., Wang, H.D., Zhou, L.T., 2020. The effect of Notch signal pathway on $PM_{2.5}$-induced Muc5ac in Beas-2B cells. Ecotoxicol. Environ. Saf. 203, 110956.

Mack, S.M., Madl, A.K., Pinkerton, K.E., 2019. Respiratory health effects of exposure to ambient particulate matter and bioaerosols. Compr. Physiol. 10, 1–20.

Maurice, N.M., Bedi, B., Yuan, Z., Goldberg, J.B., Koval, M., Hart, C.M., Sadikot, R.T., 2019. *Pseudomonas aeruginosa* induced host epithelial cell mitochondrial dysfunction. Sci. Rep. 9, 11929.

Nguyen, X.D., Zhao, Y., Evans, J.D., Lin, J., Schneider, L., Voy, B., Hawkins, S., Purswell, J.L., 2022. Evaluation of bioaerosol samplers for airborne *Escherichia coli* by poultry litter particles. J. ASABE 65, 825–833.

Nie, M., Dong, Y.H., Cao, Q., Zhao, D., Ji, S.T., Huang, H., Jiang, M.G., Liu, G.J., Liu, Y.J., 2022. CRISPR contributes to adhesion, invasion, and biofilm formation in *Streptococcus agalactiae* by repressing capsular polysaccharide production. Microbiol. Spectr. 10, e0211321.

Panas, A., Comouth, A., Saathoff, H., Leisner, T., Al-Rawi, M., Simon, M., Seemann, G., Dossel, O., Mulhopt, S., Paur, H.R., Fritsch-Decker, S., Weiss, C., Diabate, S., 2014. Silica nanoparticles are less toxic to human lung cells when deposited at the air-liquid interface compared to conventional submerged exposure. Beilstein J. Nanotechnol. 5, 1590–1602.

Raemy, D.O., Grass, R.N., Stark, W.J., Schumacher, C.M., Clift, M.J.D., Gehr, P., Rothen-Rutishauser, B., 2012. Effects of flame made zinc oxide particles in human lung cells - a comparison of aerosol and suspension exposures. Part. Fibre Toxicol. 9, 33.

Reynolds, D., Kollef, M., 2021. The epidemiology and pathogenesis and treatment of *Pseudomonas aeruginosa* infections: an update. Drugs 81, 2117–2131.

Rossy, T., Distler, T., Meirelles, L.A., Pezoldt, J., Kim, J., Talà, L., Bouklas, N., Deplancke, B., Persat, A., 2023. *Pseudomonas aeruginosa* type IV pili actively induce mucus contraction to form biofilms in tissue-engineered human airways. PLoS Biol. 21, e3002209.

Ruenraromgsak, P., Chen, S., Hu, S., Melbourne, J., Sweeney, S., Thorley, A.J., Skepper, J.N., Shaffer, M.S.P., Tetley, T.D., Porter, A.E., 2016. Translocation of functionalized multi-walled carbon nanotubes across human pulmonary alveolar epithelium: Dominant role of epithelial type 1 cells. ACS Nano 10, 5070–5085.

Saikh, S.R., Das, S.K., 2023. Fog-induced alteration in airborne microbial community: a study over central indo-gangetic plain in India. Appl. Environ. Microbiol. 89, e0136722.

Tavana, H., Kuo, C.H., Lee, Q.Y., Mosadegh, B., Huh, D., Christensen, P.J., Grotberg, J.B., Takayama, S., 2010. Dynamics of liquid plugs of buffer and surfactant solutions in a micro-engineered.pulmonary airway model. Langmuir 26, 3744–3752.

Wang, H.Y., Peng, L.H., Li, G.Y., Liu, H.L., Liang, Z.S., Zhao, H.J., An, T.C., 2024a. Enhanced catalytic ozonation inactivation of bioaerosols by MnO_2/Ni foam with abundant vacancies and at concentration. Appl. Catal. B-Environ. Energy 344, 123675.

Wang, R., Chen, R., Wang, Y., Chen, L., Qiao, J., Bai, R., Ge, G., Qin, G., Chen, C., 2019. Complex to simple: in vitro exposure of particulate matter simulated at the air-liquid interface discloses the health impacts of major air pollutants. Chemosphere 223, 263–274.

Wang, Y.N., Wang, Q.Z., Li, Y.H., Wang, B.P., Wang, H.W., Sun, Y.J., Wu, J., Li, W.H., Bian, R.X., Chen, L.J., 2024b. Insights into bioaerosol contamination in the process of mineralized refuse mining: microbial aerosolization behavior and potential pathogenicity. J. Hazard. Mater. 480, 136142.

Yao, M.S., 2022. SARS-CoV-2 aerosol transmission and detection. Eco-Environ. Health 1, 3–10.

Zhang, L., He, X., Xiong, Y., Ran, Q., Xiong, A.Y., Wang, J.Y., Wu, D.H., Niu, B., Li, G.P., 2021. Transcriptome-wide profiling discover: PM2.5 aggravates airway dysfunction through epithelial barrier damage regulated by Stanniocalcin 2 in an OVA-induced model. Ecotoxicol. Environ. Saf. 220, 112408.

Zhang, X., Ma, Z., Hao, P., Ji, S., Gao, Y., 2024. Characteristics and health impacts of bioaerosols in animal barns: a comprehensive study. Ecotoxicol. Environ. Saf. 278, 116381.

Zhao, Y., Xiong, M., Ho, K., Rao, Y., Huang, Y., Cao, J., Yue, Y., Wang, J., Wen, G., Li, J., 2024. Bioaerosol emission and exposure risk from a wastewater treatment plant in winter and spring. Ecotoxicol. Environ. Saf. 287, 117294.